Available online at www.sciencedirect.com

ScienceDirect

journal homepage: www.elsevier.com/locate/he

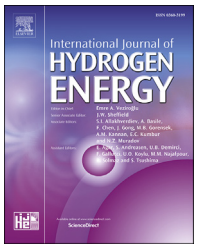

Characterization of Pt supported on commercial fluorinated carbon as cathode catalysts for Polymer Electrolyte Membrane Fuel Cell

Federico A. Viva[*], *George A. Olah*, *G.K. Surya Prakash*[**]

Loker Hydrocarbon Research Institute, Department of Chemistry, University of Southern California, Los Angeles, CA 90089-1661, USA

ARTICLE INFO

Article history:
Received 2 February 2017
Received in revised form
18 April 2017
Accepted 25 April 2017
Available online 19 May 2017

Keywords:
Carbon monofluoride (CFx)
Pt on CFx
Oxygen reduction reaction (ORR)
Polymer Electrolyte Membrane Fuel Cell (PEMFC)
Direct Methanol Fuel Cell (DMFC)

ABSTRACT

Pt nanoparticles supported on carbon monofluoride (CFx), synthesized from H_2PtCl_6 using $NaHB_4$ as a reducing agent has been investigated as a cathode electrocatalyst in fuel cells. Surface characterization, performed by transmission electron microscopy (TEM) and powder X-ray diffraction (PXRD), shows a homogeneous distribution and high dispersion of metal particles. Kinetic parameters for the electrocatalyst are also obtained from the steady state measurements using a rotating disk electrode (RDE) in 0.5 M H_2SO_4 solution. Analysis by Koutecky–Levich equation indicates an overall 4 e^- oxygen reduction reaction (ORR). Evaluation of the catalyst in single cell membrane electrode assemblies (MEAs) for proton exchange membrane based Direct Methanol Fuel Cell (DMFC) and H_2 Fuel Cell at different temperatures and flows of O_2 and Air are shown and compared against commercial Pt/C as the cathode electrocatalyst. Evaluation of Pt/CFx in H_2 fed fuel cells shows a comparable performance against a commercial catalyst having a higher platinum loading. However, in direct methanol fuel cell cathodes, an improved performance is observed at low O_2 and air flows showing up to 60–70% increase in the peak power density at very low flows (60 mL min^{-1}).

© 2017 Hydrogen Energy Publications LLC. Published by Elsevier Ltd. All rights reserved.

Introduction

Improving the performance of fuel cells (FCs) is of great interest, particularly for the PEM (Polymer Electrolyte Membrane) FC types since they hold great promise as a convenient energy source for portable applications. In PEMFC, using H_2 or other fuels, such as methanol in the case of DMFC (Direct Methanol Fuel Cell), the cathode reaction is the oxygen reduction to water for which Pt is the most active catalyst.

The materials of the different fuel cell components are selected with properties according to their function. Water management is an important factor in fuel cells [1–6] as water is necessary for the oxidation–reduction reaction and the ion transport (proton flux), affecting directly the overall performance of the fuel cell. In H_2 FCs, both H_2 and O_2 have to be humidified at anode and cathode, respectively, while in DMFC, it is not necessary to supply humidified O_2 due to large water flux (cross-over) from anode to the cathode. In any case, water management is necessary to avoid what is known as

* *Corresponding author*. Present address: Departamento de Física de la Materia Condensada, Centro Atómico Constituyentes, Comisión Nacional de Energía Atómica (CNEA), Av. General Paz 1499 (B1650KNA), San Martín, Buenos Aires, Argentina.
** *Corresponding author*.
E-mail address: viva@tandar.cnea.gov.ar (F.A. Viva).
http://dx.doi.org/10.1016/j.ijhydene.2017.04.255
0360-3199/© 2017 Hydrogen Energy Publications LLC. Published by Elsevier Ltd. All rights reserved.

compartment flooding, or cathode flooding in DMFC. To hinder flooding, the gas diffusion layer (GDL) contains a fluorinated polymer, polytetrafluoroethylene (PTFE), coating that repels water. The coating amount is chosen to exercise a precise control of the water amount, and although contact resistance of the GDL may slightly increase, the FC will keep running without significant cathode flooding.

As for the catalyst, Pt nanoparticles are supported over electrically conductive carbon in order to increase the catalyst surface area [7–11]. The carbon support plays an important role as a catalyst component. It not only provides the electrical connectivity between the metal particles and the gas diffusion layer or current collector but also the nature of the support and the interaction between support and metal particles influence the morphology, dispersion, and stability of the final catalyst [12,13], thus affecting the catalytic activity of the metal particles [8,9,14].

Fully fluorinated graphite (CFx) has been utilized in primary Li battery cathodes [15–18] and as lubricants. Fluorocarbons compounds have shown the property of having a good O_2 solubility [19–21] and among their uses include artificial blood substitutes. Recently, fluorine modified carbon was proposed as a Pt free catalyst. Sun et al. [22] doped commercial black pearls with F while Wang et al. [23] doped a prepared mesoporous carbon. Both researchers studied the ORR in basic media and Sun further employed the catalyst in alkaline direct methanol fuel cell. These works showed, as was anticipated, that the fluorine modified carbon surface might have and enhanced activity towards the oxygen reduction reaction (ORR).

The studies regarding the oxygen reduction reaction were carried out by Damjanovic [24–29] and Bockris [26–31] in the 1960, particularly on Pt single crystal. Such studies showed the complexity in studying the O_2 redox equilibrium. The exchange current density, obtained by long pre-electrolysis periods (24–48 h), (j_0) is in the order of 10^{-10} A cm^{-2} [25,32]. Another important observation derived from such studies was a change in the Tafel slope, which was interpreted as a change in the reaction kinetics under Temkin conditions at low current density to Langmuir conditions at high current densities for the electron transfer rate determining step [24,25,31,33]. Scheme 1 shows the simplified version for different reaction pathways proposed for the ORR [34]. It is well-known that in the acid media the direct 4 e^- reduction to water is the most likely pathway, while in the basic media it is possible to obtain hydrogen peroxide by a 2 e^- reduction process [29]. It is well

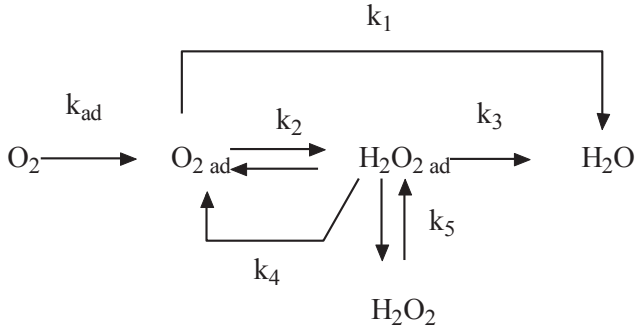

Scheme 1 – Pathway for the oxygen reduction reaction as presented by Wroblowa et al. [31].

documented that H_2O_2 degrades polymeric membranes as the ones employed in the preparation of membrane electrode assemblies (MEA) such as Nafion [35–38]. Therefore, the determination of the H_2O_2 proportion produced by cathode catalyst as well as the amount generated during the O_2 reduction inside a fuel cell was shown to be of high importance [37,38].

In the present work, we describe the use of commercially available partially fluorinated carbon monofluoride (CFx) as Pt nanoparticles support for use in PEM fuel cell cathodes. The nanoparticles were obtained by the impregnation-reduction method via $NaBH_4$ in basic media. The Pt/CFx catalyst was characterized by powder X-ray diffraction (PXRD), transmission electron microscopy (TEM), energy dispersive X-ray spectroscopy (EDS) and thermogravimetric (TG) analysis. CO stripping procedure was used for the determination of the catalyst electrochemical surface area, while the electrocatalytic activity was determined by cyclic voltammetry (CV). Kinetic as well as mechanistic parameters were obtained using the rotating disk electrode (RDE) and ring disk electrode (RRDE). Membrane electrode assemblies were fabricated using Pt/CFx as the cathode electrocatalyst and fuel cell performance obtained by feeding the cells with H_2 and methanol as fuels.

Experimental

Catalyst preparation

Slurry of the partially fluorinated CFx grade 2010, purchased from Advance Research Chemicals, Inc., was prepared by adding the predetermined amount in milli-Q water obtained from a Direct-Q3 system (Millipore), vigorously stirred and placed in an ultrasonic bath for 30 min. The CFx properties provided by the vendor are shown in SI Table 1. It is important to note that the electrical resistivity value of less than 10 Ω cm is on the same order as that of Vulcan XC-72 [39]. This is the most common carbon used to support Pt as is the case of Pt/C 40% HISPEC 4000, available from Alfa Aesar used to construct MEAs, see Sections "Electrochemical characterization and Membrane Electrode Assembly Fabrication and Fuel Cell testing". Chloroplatinic acid ($H_2PtCl_6 \cdot H_2O$ 5 g Aldrich) solution was added to the slurry in calculated amount to achieve a metal loading of 40% w/w, adjusted to pH 8 with NaOH (Pro Analysis, Aldrich) and heated to 90 °C. Once the temperature was reached, $NaBH_4$ (granular 98%, Sigma–Aldrich) was added in a molar ratio of 3:1 ($NaBH_4$ to metal) while the solution was maintained under stirring at the same temperature. After adding the $NaBH_4$, heating was continued for 2 more hours and stirring for 12 h. The mixture was transferred to a centrifuge tube, centrifuged and the solid was successively washed and centrifuged until the supernatant showed a neutral pH and absence of Cl^- by reaction with $AgNO_3$ (saturated solution). The solid was then separated and dried in a vacuum oven at 60 °C overnight.

Catalyst surface analysis

Powder X-ray diffraction (PXRD) pattern of the catalyst was obtained using a Siemens D5000 diffractometer with a Cu Kα source operating at 40 kV and 30 mA. The angle extended from 20° to 100° with a step interval of 0.02° and a counting time of

2 s. Transmission electron microscope (TEM) images of the supported catalysts were acquired with a JEOL 100CX, while energy dispersive X-ray spectroscopy (EDS) was performed using a Philips EM420 in order to quantify the amount of Pt in the catalyst. Thermogravimetric analyses (TGA) were obtained with a Shimadzu TGA-51 instrument. Supported catalyst samples (5–10 mg) were heated to 1000 °C at 5 °C per minute in a titanium crucible under air atmosphere (flow: 100 mL min^{-1}). The metal content on the supported catalysts was calculated from the difference between the initial and final weights.

Electrochemical characterization

All electrochemical experiments were performed employing a Solartron SI 1287 potentiostat/galvanostat (AMETEK). For RDE experiments, the Solartron potentiostat was coupled to a rotating ring disk electrode (Pine Research Inst.; Raleigh, NC). A silver/silver chloride (Ag/AgCl) couple was used as the reference electrode (RE) and the potentials were converted to the standard hydrogen electrode (SHE) potential. The counter electrode (CE) consisted of a coiled Pt wire of 0.5 mm in diameter and 10 cm long. A three-compartment double wall glass cell was employed in the experiments. The working electrode (WE) is introduced through the top opening in a vertical position, while at the bottom of the cell there was a glass tube with a frit in its end for sparging the desired gases. The RE compartment was connected to the main compartment by a lugging capillary while the CE compartment was separated by a frit glass from the main one. The temperature was controlled by circulating hot water using a gear pump (Cole Parmer).

For all the experiments, a suspension of the catalysts in milli-Q water and Nafion Ionomer (Aldrich, 5% in alcohol) was prepared and spread over the WE and dried in a vacuum oven at 120–140 °C for 5 min.

CO stripping and CV determination

The electrochemical surface area (ECSA) was measured by CO stripping voltammetry. The electrochemical cell was filled with 0.5 M H_2SO_4 (95–97% wt EMD. ACS grade) solution and saturated with CO (RG, AGA) for 60 min while the WE potential was maintained at 0.2 V vs. SHE. After that period, and while maintaining the potential, the solution was purged with N_2 (RG, AGA) for 15 min and two scans between 0.05 V and 1.0 V vs. SHE were completed at a scan rate of 1 mV s^{-1}.

Cyclic voltammetry (CV) measurements were performed in the presence of O_2 (RG, AGA) at room temperature in 0.1 M H_2SO_4 (95–97% wt. EMD. ACS grade) for three different electrocatalysts, namely Pt/CFx prepared in section "Catalyst preparation"; Pt/C 40% wt. (Alfa Aesar HiSPEC 4000); and Pt black (Alfa Aesar HiSPEC 1000). Before each measurement, the H_2SO_4 solution was deaerated by purging Ar, followed by saturation with O_2 for 15 min. CVs were performed at 5 mV s^{-1} with an O_2 flow of 8 mL min^{-1}.

For both measurements mentioned above, the working electrode (WE) consisted of a graphite disc (Aldrich 99%) mounted on a Teflon rod where only one of the circular faces of 1 cm^2 area was exposed, the exposed face was sanded with 200 grit paper to get a rough surface before being covered with the catalyst paint. The amount of dry catalyst over the electrode was ca. 1 mg.

Oxygen reduction measurement by RDE and RRDE

Oxygen reduction experiments were performed using a rotating glassy carbon disk electrode (0.196 cm^2) – platinum ring electrode (Pine Research Inst.; Raleigh, NC). The amount of catalyst over the electrode used maintained the same ratio of 1 mg cm^{-2} as in the previous section. RDE and RRDE measurements were performed in the temperature range from 288 K to 303 K, in 0.5 M H_2SO_4 aqueous media, and efficiency parameters were calculated by means of Tafel's plots. Voltammograms were recorded for the ORR at different rotation speeds (ω = 100–2500 rpm). The potential was scanned between 1.1 and 0 V (vs. SHE) at 5 mV s^{-1}. The calibration of the RRDE was carried out by measuring the disk (I_{disk}) and ring (I_{ring}) currents in a 0.005 M $K_3Fe(CN)_6$ + 0.1 M K_2SO_4 aqueous electrolyte solution. The disk potential was cycled between 0.0 and 1.0 V at 5 mV s^{-1}, while the ring potential was fixed at 1.4 V in order to oxidize the Fe^{+3} generated in the disk. This procedure was repeated at different rotating speeds. The RRDE collection efficiency (N) was determined from the slope of disk current vs. ring current plots yielding a value of 0.20 [40].

Membrane electrode assembly fabrication and fuel cell testing

MEAs for H_2 FC and DMFC were prepared by a direct catalyst paint method onto the gas diffusion electrode (GDE). Pt/Ru 50-50 (HiSPEC 6000, Alfa Aesar) was used on the anode of DMFC, while Pt black was used for the H_2 FC. For the cathode of both DMFC and H_2 FC, only Pt/CFx and Pt/C 40% wt (Fuel cell Store) were used. Suspension of the catalysts for the anode and cathode were prepared by mixing the corresponding catalyst with milli-Q water and Nafion Ionomer (Aldrich, 5% in alcohol). The suspension was prepared in a mass ratio of 1:3:1 (catalyst–water–ionomer) for DMFC and 1:3:5 (catalyst–water–ionomer) for H_2 FC. Catalyst suspension was spread on one side of a 25 cm^2 Toray C paper TGP-H60 10% wet proofing (E-TEK). Final electrode loading for the cathode was ca. 4 mg cm^{-2} for DMFC and 1 mg cm^{-2} for H_2 FC, while the anode had a slightly higher loading than the cathode to avoid being the one limiting the performance of the fuel cell. The final Nafion weight percent in the catalyst layer was 4.8% for DMFC and 20% for H_2 FC at each electrode. Nafion 117 (Ion Power), previously treated by boiling the membrane in H_2O_2 3% (H_2O_2 30%, VWR International) followed by boiling it in 3% aqueous H_2SO_4 solution, was placed in between the electrodes and hot pressed at 150 °C and 500 kg force for 50 min. After rehumidification of the MEA by circulating water in the assembled fuel cell overnight at 80 °C, it was tested using a Fuel Cell Test System 890B from Scribner Associated.

Results and discussions

Catalyst surface characterization

TEM images of the Pt/CFx with the particle size distribution are presented in Fig. 1 (and inset). The average particle size obtained for Pt/CFx was 4.5 nm with a median of 4.6 nm. Some nucleation of the Pt over the CFx was also observed, but overall, the Pt was well dispersed with a homogeneous particle size.

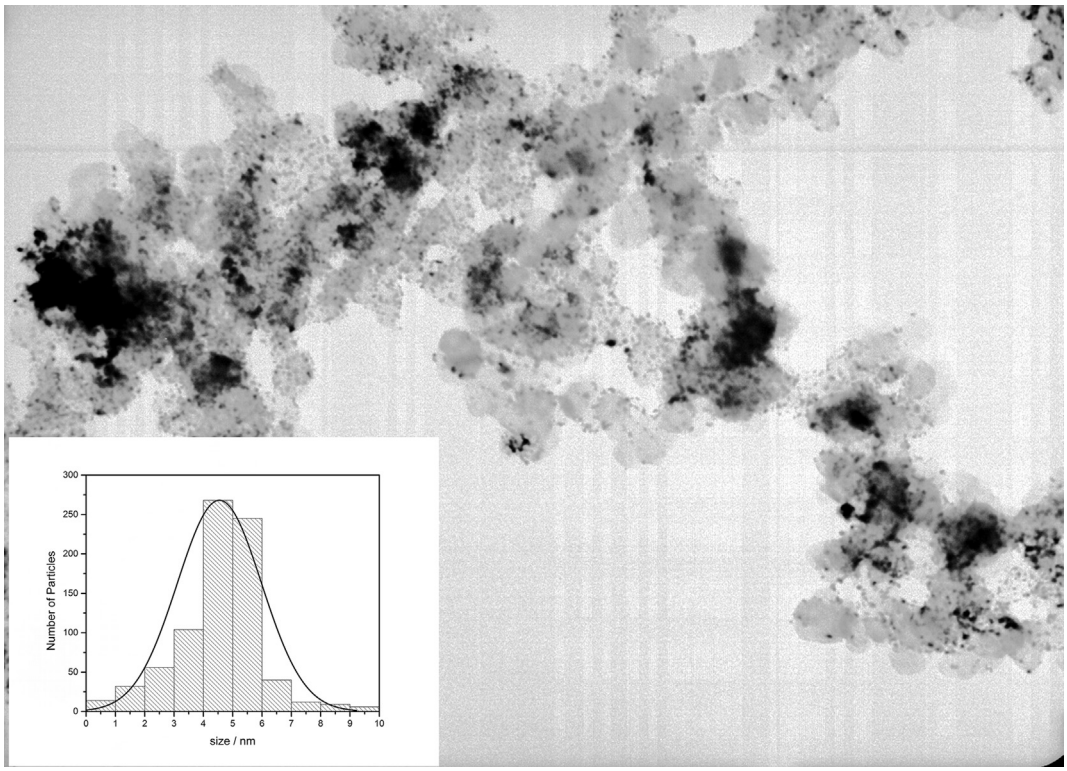

Fig. 1 – TEM image at 20,000×. Inset: Histogram of particle size distribution of Pt/CFx.

EDS analysis was performed in order to confirm the presence of Pt and to quantify the amount on the catalyst, showing a 34% Pt by weight. The F content of CFx provided by the manufacturer (~10% w) was used as an internal standard. The Pt amount was also assessed by TGA, wherein a 31% w. was found.

The PXRD patterns of the prepared catalyst, CFx and commercial Pt/C are shown in Fig. 2. The CFx diffractogram shows two peaks around $2\theta = 25°$ and $2\theta = 43°$. Previous reports have shown mainly two peaks for fluorinated carbons [18], one around $2\theta = 13°$ assigned to the (002) plane for highly fluorinated carbons and one at $2\theta = 41°$ assigned to (100) plane.

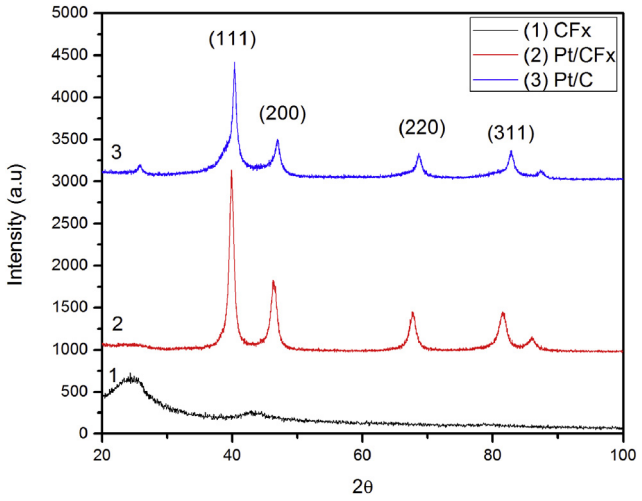

Fig. 2 – PXRD patterns of CFx, Pt/CFx, and commercial Pt/C (Alfa Aesar HiSPEC 4000).

In the present work, 2θ was started at 20° and therefore the (002) plane was not observed, while the corresponding (100) plane was present. The peak around $2\theta = 13°$ could be related to the (002) shifted to higher values due to the low fluorination degree of the present CFx material. The Pt/CFx diffractogram shows the characteristic diffraction peaks of face centred cubic (fcc) crystalline Pt, corresponding to the planes (111), (200), (220) and (311). The lattice parameter was calculated by indexing the first three peaks, i.e. (111)-(200)-(220) yielding a value of 3.91 ± 0.01 Å, while the crystal size, calculated using Scherrer's formula, gave a value of 5.3 ± 0.5 nm. The peaks corresponding to the diffractogram of Pt/C are wider than those of Pt/CFx indicating smaller crystallites as expected by the lattice value reported at 4.5 nm [40].

Electrochemical measurements

CO stripping and CV results

The CO stripping voltammetry of Pt/CFx is shown in SI Fig. 1. Electrochemical surface area (ECSA) was calculated based on the catalyst amount deposited onto the WE and the peak integration using the reference charge value of 420 μC cm^{-2} for the oxidation of a CO monolayer [41]. The calculated ECSA obtained was 56 m^2 g^{-1}.

Fig. 3 shows the voltammograms in oxygen saturated 0.1 M H_2SO_4 solution for Pt/CFx, Pt/C 40% wt., and Pt black. The values of the ECSA were used to convert current (i) to current density (j). Johnson Matthey reports a value of 60 m^2 g^{-1} for the Pt/C 40% (HiSPEC 4000) and 27 m^2 g^{-1} for Pt black (HiSPEC 1000) [40,42]. CVs for the three catalysts showed that the absolute current density value for the O_2 reduction peak was higher for

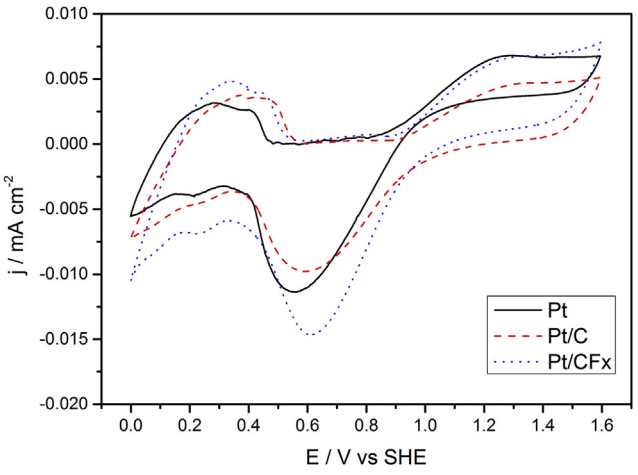

Fig. 3 – Cyclic voltammogram of catalysts in H_2SO_4 0.1 M at 5 mV s^{-1} and 298 K with an O_2 flow of 8 mL min^{-1}.

the Pt/CFx indicating a higher activity for the reduction process. The cathodic peak potential for Pt/CFx is more anodic than Pt/C and Pt and their values being 0.41, 0.40 and 0.36 V, respectively, indicative of a lower overpotential for the oxygen reduction. This is also indicated by the onset potentials, where Pt/CFx presents a value of about 100 mV more anodic than the other two catalysts. Additionally, the peaks observed in the H adsorption/desorption region of the CVs are more defined for the Pt/CFx than for Pt/C, indicating a more defined surface structure for the former [43].

ORR analysis by RDE

The overall measured current density (j) of the oxygen reduction can be expressed in terms of the kinetic current density (j_k) and the diffusion limited current density (j_d) by the Koutecky–Levich (KL) equation [42]:

$$\frac{1}{j}=\frac{1}{j_k}+\frac{1}{j_d}=\frac{1}{j_k}+\frac{1}{B\omega^{1/2}} \quad (1)$$

where,

$$B = 0.2nFC_oD_o^{2/3}\nu^{-1/6} \quad (2)$$

where 0.2 is a constant used, when the rotation speed, ω, is expressed as rpm, n is the number of electrons transferred per molecule of O_2 reduced, F the Faraday constant, C_o is the concentration of oxygen dissolved (1.1×10^{-6} mol cm^{-3}), D_o is the diffusion coefficient of oxygen in the solution (1.4×10^{-5} cm^2 s^{-1}), and ν the kinematic viscosity of the 0.5 M H_2SO_4 solution (1.0×10^{-2} cm^2 s^{-1}) (298 K) [44]. It is possible to calculate the theoretical slope of the KL plot (log j vs. $\omega^{-1/2}$) considering a four electrons reduction process, i.e., a complete reduction of O_2 to H_2O. The oxygen concentration and diffusion coefficient dependence with temperature were taken into account for corrections of the theoretical 4 electrons K–L plots using the values reported in the literature [45].

The current density–potential curves at different rotation speeds, obtained in O_2 saturated 0.5 M H_2SO_4 solution at 293 K are shown in Fig. 4. They exhibit a well-defined charge-transfer kinetic control, mixed kinetic-diffusion, and diffusion-limited currents. A similar behavior was found for the density–potential curves measured at other temperatures. A slight diffusion of the oxygen close to 0.8 V can be observed at 100 and 200 rpm. Although this behavior could be a result of the amount of catalyst used over the electrode, experiments carried out with loadings in the order of 10 μg cm^{-2} showed the same performance. In the report by Sun et al. [22] the lowest rotation speed employed was 225 rpm and no diffusion can be observed, however in the work by Wang and Kong [23] the lowest rotation applied was 625 rpm, a slight diffusion can be observed and is plausible that at lower rotation rates the diffusion might be higher. Nonetheless, further experiments need to be conducted in order to elucidate such observations.

The slopes of the KL plot (inset B Fig. 4), obtained from the mass-transfer corrected current, were used to calculate the number of electrons involved in the ORR. The experimental value obtained was 9.49×10^{-2} mA^{-1} cm^2 $rpm^{1/2}$ corresponding to an n value of 3.97, the theoretical calculated slope, considering also a 4 e^- process, is 9.41×10^{-2} mA^{-1} cm^2 $rpm^{1/2}$ lead to the conclusion that the ORR on Pt/CFx catalyst follows a 4 electron charge transfer process to water formation under the acidic conditions. Between 0.3 V and 0.6 V, the lines were quite parallel, indicating the independence of the active surface with the potential applied. The reaction order was further evaluated by plotting log j vs log $(1-j)\, j_d^{-1}$, shown in Fig. 4 inset C. The slope (m) of the intersecting lines indicates a value, in all cases, close to 1 confirming a first-order dependence of the kinetics of the adsorbed oxygen on the Pt/CFx surface. Both results indicate that the oxygen reduction proceeds via an overall four-electron transfer reaction with protons to form water.

Tafel analyses were also performed at temperatures between 288 and 303 K, in order to obtain information of the reduction mechanism of the Pt/CFx through the Tafel's slope (b) and exchange current density (j_0). As was stated in the introduction, Damjanovic et al. observed a change in the Tafel slope from a value of RT F^{-1} (59 mv dec^{-1}) for low current density under Temkin condition to a value of 2RT F^{-1} (118 mV dec^{-1}) for high current density under Langmuir condition [25,33]. Furthermore, it was shown that the mechanism proposed by the authors for crystalline Pt also apply for polycrystalline Pt [46] and the values measured can depend on the experimental conditions, particularly for the Tafel slope [47].

The mass transfer corrected Tafel plots at the studied temperatures are shown in SI Fig. 2. A linear behavior in the mixed activation-diffusion region was observed as well an increase of the current density with temperature. Tafel's parameters, obtained from Tafel plots, are summarized in Table 1. The exchange current density (j_0) and Tafel slope (b) was evaluated as a function of temperature, taking into consideration of the reversible oxygen electrode potential, E_r, at each temperature. The dependence of E_r on temperature was evaluated using the Nernst equation:

$$E_r = -\Delta G^0_{(H_2/O_2)}\Big/2F \quad (3)$$

with the following temperature dependence [48] for $\Delta G^0_{(H_2/O_2)}$:

$$\Delta G^0_{(H_2/O_2)}\,(J\ mol^{-1}) = -296,658 - 33.6T\ln T + 389.8T \quad (4)$$

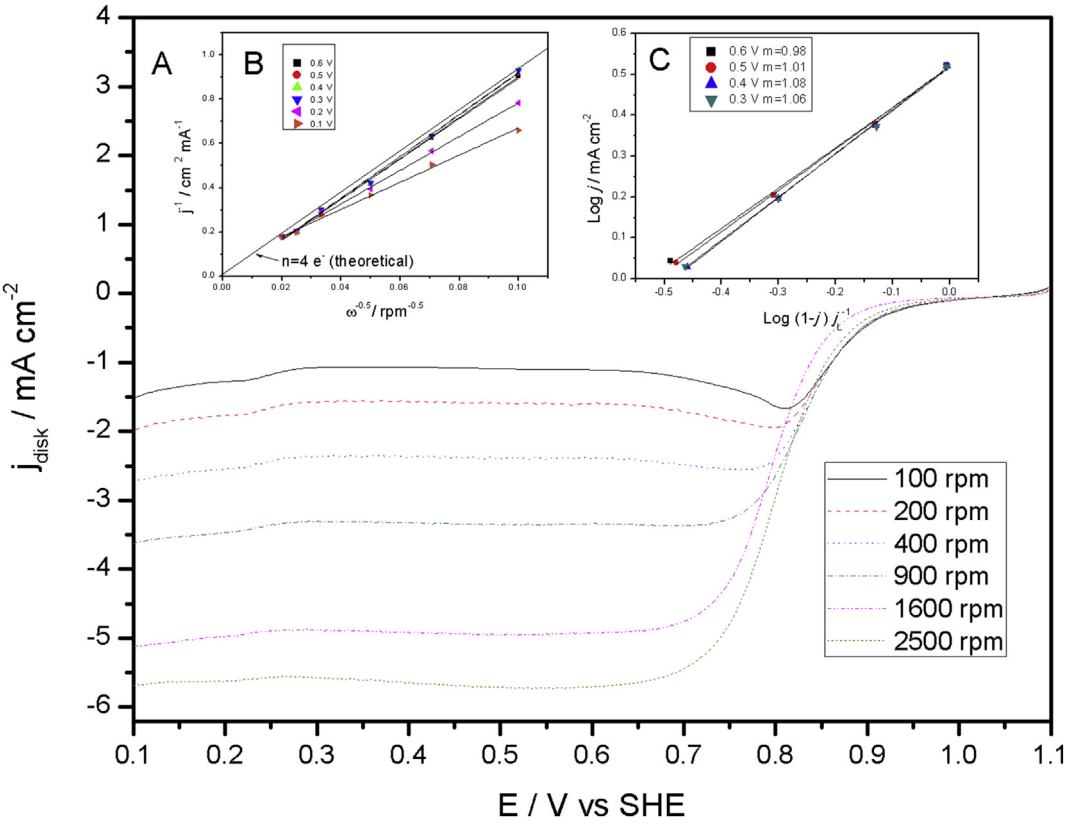

Fig. 4 – A: Rotating disk voltammograms at various rotation rate for Pt/CFx at a scan rate of 5 mV s^{-1} in O_2 saturated 0.5 M H_2SO_4 at 293 K. B: Koutecky–Levich plots obtained from the rotating disk voltammograms. C: reaction order determined from the rotating disc voltammograms.

The value obtained for *b* is ca. 110 mV dec^{-1}, close to the value of 2RT F^{-1} as reported by Damjanovic et al. [28,33], while for j_0 the increase with temperature was noticeable as the value order agrees with the reported values [28,32,33]. The temperate dependence of j_0 was employed to obtain the apparent enthalpy of activation $\Delta H^{\#}$ by plotting log j_0 vs T^{-1} following the Arrhenius equation (5) as shown in the inset of SI Fig. 2:

$$\frac{\partial \log j_0}{\partial T^{-1}} = -\frac{\Delta H^{\#}}{2.303R} \quad (5)$$

A value of 36.3 kJ mol^{-1} was obtained for the apparent enthalpy of activation falling in the range of 20–60 kJ mol^{-1} reported for nanostructured Pt and Pt based electrocatalysts [49,50].

Table 1 – Values of the kinetics parameters obtained from Tafel plots for Pt/CFx in 0.5 M H_2SO_4 at the temperatures evaluated.

Temperature (K)	b (mV dec^{-1})	j_0 (A cm^{-2})
288	107	1.71×10^{-4}
293	107	2.17×10^{-4}
298	107	2.73×10^{-4}
303	109	3.57×10^{-4}

ORR analysis by RRDE

The RRDE analysis allows the calculation of the H_2O_2 percentage generated during the O_2 reduction, through pathway k_2 (Scheme 1), using the equation [50]:

$$\%H_2O_2 = \frac{200 \times j_{ring}/N}{j_{disk} + j_{ring}/N} \quad (6)$$

where *N* is the experimental collection efficiency indicated in section "Oxygen reduction measurement by RDE and RRDE". Fig. 5 depicts the disc (j_{disk}) and the ring (j_{ring}) currents densities vs. the disc potential obtained in RRDE experiments for the Pt/CFx at the different rotation rates. The percentage of H_2O_2 produced as a function of the electrode disc potential at different electrode rotation speeds at 293 K is shown in SI Fig. 3. The maximum amount of H_2O_2 is ca. 0.5% for rotating speeds of 100 and 200 rpm below 0.2 V vs SHE. This result indicates that the ORR on Pt/CFx proceeds mostly to water, with a yield of >99%, following preferentially a 4 electron transfer reaction mechanism. The formation of H_2O_2 is very low, although not negligible, and shows a clear dependence on the applied potential. The increase of H_2O_2 formation observed at low potential was reported to be due to the oxygen reduction over the carbon support [40,46]. In the present work, the low amount of H_2O_2 generated over the PtCFx is remarkable compared to the amount usually reported (2–4%) for supported Pt on carbon [51]. It was shown [25,40] that the

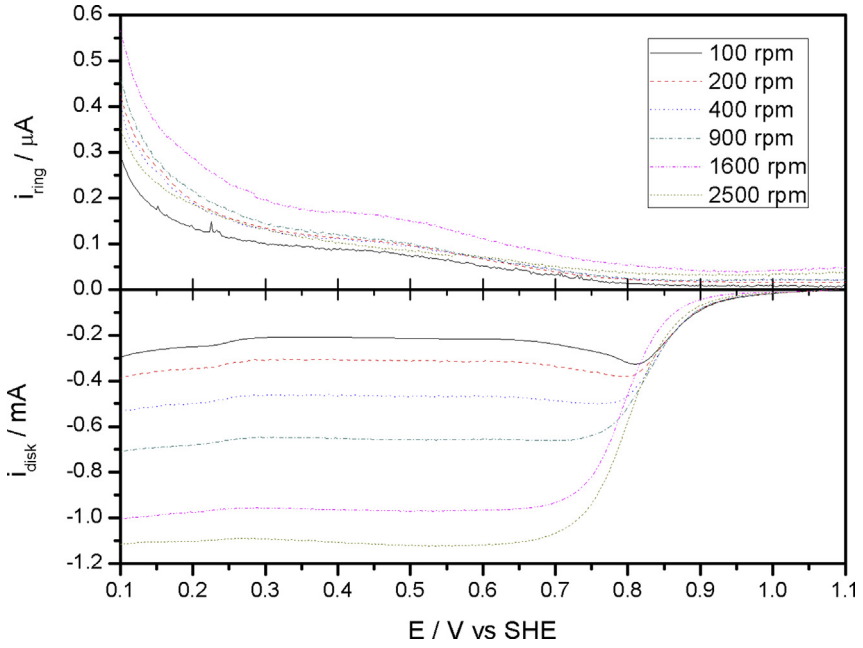

Fig. 5 – Disk and ring electrodes linear voltammograms at various rotation rates for Pt/CFx at a scan rate of 5 mV s^{-1} in O_2 saturated 0.5 M H_2SO_4 at 293 K.

relationship between the disk and ring currents also provides information on the influence of the different reaction pathways in the overall reaction mechanism (Scheme 1). The plot of $j_{disk}\, j_{ring}^{-1}$ vs. $\omega^{-0.5}$, shown in the inset of SI Fig. 3, correspond to a reaction mechanism where $k_1 \neq 0$ and $k_3 = 0$ [40]. The plot does not give any information about the reaction pathway for H_2O_2 formation. However, from the data presented, it can be concluded that on Pt/CFx the amount of H_2O_2 formed is low, which is produced mainly by the catalyst carbon support and does not further proceed to the formation of H_2O ($k_3 = 0$).

Single cell fuel cell testing

After assembly of the MEAs, re-humidification and conditioning by fast galvanodynamic scan, resistance of the fuel cell was measured with a milliohmmeter (Hewlett Packard, model 4338B). The cell resistance was used to asses problems occurring during MEA pressing or FC conditioning process. All the MEAs showed similar values, ca. 15 mΩ, of resistance for both Pt/CFx and Pt/C based cathodes.

Pt/CFx evaluation in H_2 FC

MEAs prepared for H_2 FC were tested at 90 °C by feeding fully humidified (100% RH) H_2 and O_2 at the anode and cathode respectively, at different flow values and with no back pressure. Data are presented in Fig. 6(A and B). The data obtained in Fig. 6(A) corresponds to a flow of 600 mL min^{-1} for H_2 and 700 mL min^{-1} for O_2. While in Fig. 6(B), the flows values are 300 mL min^{-1} for H_2 and 400 mL min^{-1} for O_2, being the last set of the lowest flows tested. Once the gases were circulated through the cell, the FC with Pt/CFx attained at optimal OCV value of ca. 1.0 V as with the commercial catalyst. The performance shown by the Pt/CFx is comparable to the performance of the commercial catalysts being slightly better for the Pt/CFx at the lowest flow set. The charge transfer resistance for Pt/CFx is lower than for the Pt/C for both flow sets, as shown by the initial drop in voltage at low current density, in the activation polarization zone. The ohmic polarization and mass transfer polarization zone of the curve are similar for both cathode catalyst, showing that the properties of Pt/CFx do not differ considerably from Pt supported on a regular carbon. It is interesting to notice that the peak current density for Pt/C is 350 mW cm^{-2} for the high flow set and 300 mW cm^{-2} for the low flow set, while for PtFCx the peak current density increases from 325 mW cm^{-2} to 350 mW cm^{-2} when changing from the high flow set to the low flow set. As indicated in section "Catalyst surface characterization", the amount of Pt over CFx is lower than in the Pt/C, hence the polarization curves indicate a better performance for the former.

Pt/CFx evaluation in DMFC

MEAs for DMFC were tested with aqueous 1 M methanol solution at 90 °C, 60 °C, 30 °C, with O_2 flows ranging from 1.2 L min^{-1} to 40 mL min^{-1} and air from 1.3 L min^{-1} to 200 mL min^{-1}. Both gases were used dry and no back pressure was employed at the cathode.

At O_2 flows above 400 mL min^{-1}, the performance and power densities of the cell with Pt/C on the cathode were higher than the ones shown by Pt/CFx. However, when the O_2 flow was decreased, major improvement of Pt/CFx performance was observed, while the performance of Pt/C decreased steadily. At 700 mL min^{-1}, the Pt/C performance was still above the Pt/CFx as presented in Fig. 7. Fig. 8(A and B) shows the performance of the cathode catalyst at 200 and 60 mL min^{-1} of O_2 flow, respectively, with 1 M methanol at 90 °C. When the O_2 flow was decreased to 200 mL min^{-1}(Fig. 8A), Pt/CFx not only showed better performance than Pt/C but also the performance was better than for the same catalyst at higher O_2 flow rate. The

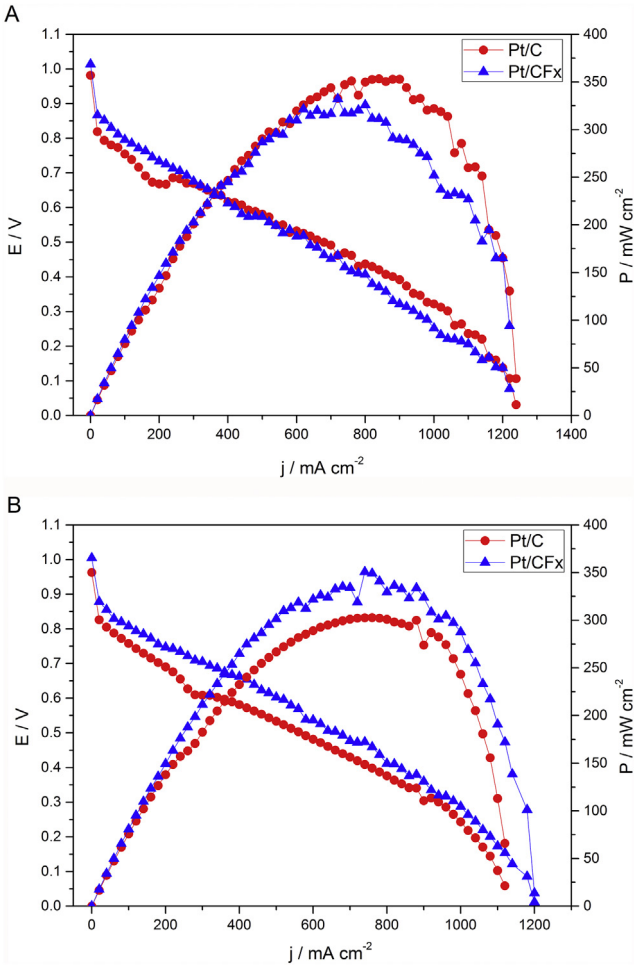

Fig. 6 – Polarization and power plot for Pt/C and Pt/CFx at 90 °C. A: H_2 flow of 600 mL min^{-1} and 700 mL min^{-1} for O_2. B: H_2 flow of 300 mL min^{-1} and 400 mL min^{-1} for O_2.

power density for PtCFx shows a maximum of 55 mW cm^{-2} for an O_2 flow of 200 mL min^{-1}. Such value is higher than the peak power obtained for the same catalyst at 700 mL min^{-1}. Such behavior is uncommon as typically the performance of the cell decreases when the fuel or the oxidant, as in this case, is being decreased. Moreover, the value is similar for the value of

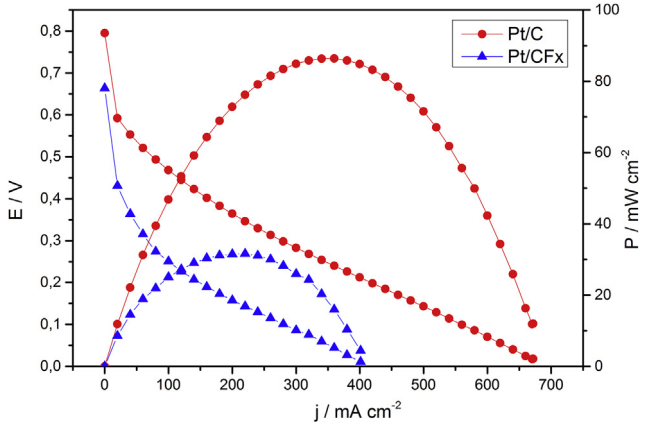

Fig. 7 – Polarization and power plot for Pt/C and Pt/CFx with 1 M methanol at 700 mL min^{-1} of O_2 and 90 °C.

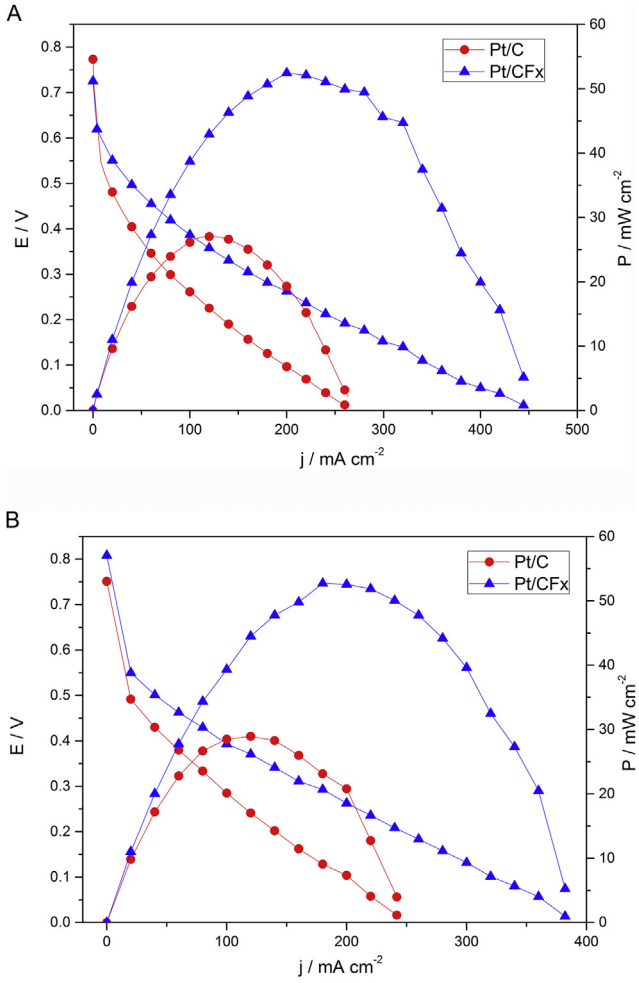

Fig. 8 – Polarization and power plot for Pt/C and Pt/CFx with 1 M methanol at 90 °C. A: O_2 flow at 200 mL min^{-1}. B: O_2 flow at 60 mL min^{-1}.

60 mW cm^{-2} of PtC at 400 mL min^{-1} (not shown) and 60% of the value observed for 700 mL min^{-1} (Fig. 7). The same trend as for 200 and 60 mL min^{-1} of O_2 flows was obtained at an O_2 flow rate of 40 mL min^{-1}. Measurements at 60 °C and 30 °C showed that Pt/CFx had the same performance as the Pt/C even at an O_2 flow rate of 1.2 L min^{-1}, in contrast with 90 °C, and a better performance was observed above 400 mL min^{-1}. SI Fig. 4(A and B) shows the performance for O_2 flow of 60 mL min^{-1} at 60 °C and 30 °C, respectively, where Pt/CFx presented a peak power density of 53 and 23 mW cm^{-1}. As for the low flow set at 90 °C, the performance of Pt/CFx was better than that of the Pt/C. Comparison of all the above mentioned figures for the different O_2 flows and temperatures indicates that the performance for Pt/CFx does not decrease as abruptly as the commercial catalyst does when the flow O_2 is decreased. SI Fig. 5(A and B) shows the data obtained for Pt/CFx and Pt/C tested with 1 M methanol and air flow of 760 mL min^{-1} at 90 °C and 60 °C, respectively. The figures are representative of the different conditions evaluated with air. Similar to the results obtained employing O_2 at the cathode, the performance of Pt/CFx was above than that of the commercial Pt/C starting at higher flow conditions (760 mL min^{-1}) than for the measurements with O_2.

Similar to what was observed with the MEAs evaluated with H_2, the OCV reached a typical value for DMFC of ca. 0.7–0.8 V as soon as methanol and O_2 reached the cell. As can be observed, the shape of the polarization varies slightly with the different conditions, nonetheless no negative behavior is observed for the activation or ohmic polarization. Long term performance experiments were not carried out for the Pt/CFx, however the cell for both cathode catalyst was run and evaluated on a daily basis for a period of twenty days. In that period, no observable decrease in the performance was observed for either catalyst. SI Fig. 6 shows the performance for Pt/CFx and Pt/C with 1 M methanol and 700 mL min^{-1} of O_2 at 90 °C for the initial and final day of tests. The performance for both catalyst after 20 days of experiments is even slightly better than the first day. Although the fuel cell conditioning strives to shorten the period in which the performance reaches a maximum, such behavior is not uncommon as the performance could improve slightly as the cell is polarized.

Conclusion

The preparation of a Pt catalyst supported on partially fluorinated CFx by chemical reduction has been carried out and its performance analyzed. The fluorine-modified carbon does not hinder the deposition and formation of Pt nanoparticle as shown by the TEM and XRD. The electrochemical measurements, particularly RDE shows that there was no change in the oxygen reduction mechanism for the Pt supported over CFx and that the amount of H_2O_2 produced is minuscule under the acidic conditions. The catalyst was assessed in the cathode of single cell fuel cells. In DMFC, for a given set of conditions, the performance in terms of the polarization and power plot were better for Pt/CFx than the other catalyst tested. The improvements are seen particularly at low O_2 and air flows. In H_2 FC, only few experiments were conducted and although the improvement of Pt/CFx over Pt/C is not as noticeable as in DMFC there is an improvement at the lowest O_2 flow rates, particularly considering the lower amount of Pt on the catalyst. Although the electrochemistry shows no clear difference between the Pt supported onto regular carbon and CFx, the performance in the fuel cell environment is clearly better at lower oxidant flow sets. Results obtained from CV and RDE does not provide explanation on why low flow set render better performance. Nevertheless, it is possible that the fluorinated surface of the carbon extends the residence time of O_2 as if flows through the cell compartment improving the reaction kinetics. Further experiments need to be carried out to understand why the high flows present a decreased performance. Nonetheless, it can be concluded that partially fluorinated CFx is an interesting option as an ORR catalyst support particularly for the purpose of decreasing the amount of Pt in FC cathodes.

Acknowledgments

Support of the work by the Loker Hydrocarbon Research Institute at USC is gratefully acknowledged. FAV is currently a research fellow of CICyT of CONICET (Argentina).

In memory of GAO who passed away on March 8, 2017

Appendix A. Supplementary data

Supplementary data related to this article can be found at http://dx.doi.org/10.1016/j.ijhydene.2017.04.255.

REFERENCES

[1] Wang G, Sun G, Zhou Z, Liu J, Wang Q, Wang S, et al. Electrochem Solid State Lett 2005;8:A12–6.
[2] Lu GQ, Liu FQ, Wang C-Y. Electrochem Solid State Lett 2005;8:A1–4.
[3] Xie F, Tian Z, Meng H, Shen PK. J Power Sources 2005;141:211–5.
[4] Kunimatsu M, Okada T. Electrochem Solid State Lett 2004;7:A389–90.
[5] Scott K, Argyropoulos P. J Power Sources 2004;137:228–38.
[6] Zhong C-J, Luo J, Njoki PN, Mott D, Wanjala B, Loukrakpam R, et al. Energy Environ Sci 2008;1:454–66.
[7] Auer E, Freund A, Pietsch J, Tacke T. Appl Catal A 1998;173:259–71.
[8] Liu H, Song C, Zhang L, Zhang J, Wang H, Wilkinson D. J Power Sources 2006;155:95–110.
[9] Pantea D, Darmstadt H, Kaliaguine S, Roy C. Appl Surf Sci 2003;271:181–93.
[10] Pantea D, Darmstadt H, Kaliaguine S, Summchen L, Roy C. Carbon 2001;39:1147–58.
[11] Higgins D, Zamani P, Yu A, Chen Z. Energy Environ Sci 2016;9:357–90.
[12] Cui Z, Liu C, Liao J, Xing W. Electrochim Acta 2008;53:7807–11.
[13] Zhou WJ, Li WZ, Song SQ, Zhou ZH, Jiang LH, Sun GQ, et al. J Power Sources 2004;131:217–23.
[14] Delafuente J, Martinezhuerta M, Rojas S, Terreros P, Fierro J, Pena M. Catal Today 2006;116:422–32.
[15] Watanabe N, Morigaki K. Denki Kagaku 1979;47:169–73.
[16] Whitacre JF, West WC, Smart MC, Yazami R, Prakash GKS, Hamwi A, et al. Electrochem Solid State Lett 2007;10:A166–70.
[17] Ma Z, Yuan X, Li L, Ma Z-F, Wilkinson DP, Zhang L, et al. Energy Environ Sci 2015;8:2144–98.
[18] Zhang Q, Takeuchi KJ, Takeuchi ES, Marschilok AC. Phys Chem Chem Phys 2015;17:22504–18.
[19] Hamza MA, Serratrice G, Stebe MJ, Delpuech JJ. J Am Chem Soc 1981;103:3733–8.
[20] Lawson DD, Moacanin J, Scherer KV, Terranova TF, Ingham JD. J Fluor Chem 1978;12:221–36.
[21] Wesseler EP, Iltis R, Clark LC. J Fluor Chem 1977;9:137–46.
[22] Sun X, Zhang Y, Song P, Pan J, Zhuang L, Xu W, et al. ACS Catal 2013;3:1726–9.
[23] Wang H, Kong A. Mater Lett 2014;136:384–7.
[24] Damjanovic A, Genshaw MA. Electrochim Acta 1970;15:1281–3.
[25] Damjanovic A, Brusic V. Electrochim Acta 1967;12:615–28.
[26] Damjanovic A, Genshaw MA, Bockris JOM. J Electrochem Soc 1967;114:466.
[27] Damjanovic A, Genshaw MA, Bockris JOM. J Phys Chem 1966;70:3761.
[28] Damjanovic A, Dey A, Bockris JOM. J Electrochem Soc 1966;113:739.
[29] Damjanovic A, Genshaw MA, Bockris JOM. J Electrochem Soc 1967;114:1107.
[30] Bockris JOM, Huq AKMS. P R Soc 1956;237A:1733.
[31] Wroblowa H, Rao MLB, Damjanovic A, Bockris JOM. J Electroanal Chem 1967;15:139.
[32] Damjanovic A, G HP. J Electrochem Soc 1988;135:2269–73.

[33] Damjanovic A, Sepa DB, Vojnovic MV. Electrochim Acta 1979;24:887–9.
[34] Wroblowa HS, Yen Chi P, Razumney G. J Electroanal Chem 1976;69:195–201.
[35] Pianca M, Barchiesi E, Esposto G, Radice S. J Fluor Chem 1999;95:71.
[36] Curtin DE, Lousenberg RD, Henry TJ, Tangeman PC, Tisack ME. J Power Sources 2004;131:41.
[37] Liu W, Zuckerbrod D. J Electrochem Soc 2005;152:A1165.
[38] Schmittinger W, Vahidi A. J Power Sources 2008;180:1–14.
[39] Cabot Specialty Carbon Blacks. http://www.cabot-corp.com/Specialty-Carbon-Blacks/Products?recOffset=80 [accessed 10/2011].
[40] Lee SJ, Pyun SI, Lee SK, Kang SJL. Isr J Chem 2008;48:215–28.
[41] Bockris JOM, Kahn SUM. Surface electrochemistry. New York: Plenum; 1993.
[42] Bard AJ, Faulkner LR, editors. Electrochemical methods. Fundamentals and applications. 1st ed. J. Wiley & Sons; 1980.
[43] Markovic NM, Ross PN. Surf Sci Rep 2002;45:121–229.
[44] Couteanceau C, Crouigneau P, Léger JM, Lamy C. J Electroanal Chem 1994;389.
[45] Lide DR. CRC handbook of chemistry and physics. 90th ed. CRC; 2009.
[46] Antoine O, Bultel Y, Durand R. J Electroanal Chem 2001;499:85–94.
[47] Sepa DB, Vracar LM, Vojnovic MV, Damjanovic A. Electrochim Acta 1986;31:1401–2.
[48] Suárez-Alcántara K, Solorza-Feria O. Fuel Cells 2010;10:84–92.
[49] Mukerjee S, Srinivasan S, Soriaga MP, McBreen J. J Phys Chem 1995;99:4577–89.
[50] Paulus UA, Schmidt TJ, Gasteiger HA, Behm RJ. J Electroanal Chem 2001;495:134–45.
[51] Benítez R, Chaparro AM, Daza L. J Power Sources 2005;151:2–10.